The International Journal of Materials and Engineering Technology (TIJMET) (2024) 7(2)
http://dergipark.gov.tr/tijmet
ISSN: 2667-4033

RESEARCH ARTICLE https://doi.org/10.70858/tijmet.1541458

Experimental and numerical investigation of the use of organic and inorganic materials melted with infrared rays for thermal energy storage

Ali Kemal Özcan*[1], Ömer Öksüz[2] and Cevdet Demirtaş[2]

[1]*Karadeniz Technical University, Graduate School of Natural and Applied Science, Trabzon, Türkiye*
[2]*Karadeniz Technical University, Faculty of Engineering, Department of Mechanical Engineering, Trabzon, Türkiye*

Article Info

Article history:
Received 12.09.2024
Revised: 26.12.2024
Accepted: 30.12.2024
Published Online: 31.12.2024

Keywords:
Infrared rays
Paraffin
Hitec salt
Thermal storage

Abstract

Energy storage processes need to be researched and developed to ensure the conversion and sustainability of energy. The original value of this study lies in the experimental and numerical investigation of the performance of an innovative heat storage system using infrared radiation and phase change materials (PCMs). In a laboratory setting, infrared rays emitted by a lamp are directed through a conical concentrator onto organic as paraffin and inorganic Hitec salts. These materials are melted and analyzed for their potential use in thermal energy storage. During a 4-hour charging process, the focal temperature ranged between 200–300°C. The maximum temperatures measured in the upper region of a 10-liter furnace were 87°C for paraffin and 240°C for Hitec salts. In the subsequent 4-hour discharge process, the upper region temperature of the Hitec salt decreased from approximately 102°C to 46°C, while the paraffin's temperature dropped from 75°C to 55°C. With mass flow rates of 0.047 g s^{-1} for paraffin and 0.061 g s^{-1} for Hitec salt, the average thermal efficiencies in the furnace were calculated as 56% for paraffin and 65.6% for Hitec salts. The first-law thermodynamic efficiencies were determined to be 8% for paraffin and 19.7% for Hitec salts. In summary, paraffin is ideal for low-temperature applications (below 80°C), while Hitec salts are more suitable for medium to high-temperature applications due to their superior thermal properties.

1. Introduction

There are many different energy production methods to meet the demand for energy consumption. The demand for renewable and sustainable energy production and energy storage methods is increasingly increasing. Innovative energy storage methods are being researched and implemented to ensure continuity and diversity in energy. Thermal energy storage studies are also increasing with the point heat source created by concentrating solar energy, which is one of the renewable energy sources. Thermal energy is provided with infrared lamps to ensure continuity in cases where there is no solar energy. The phase change materials used in thermal energy storage consist of organic, inorganic and eutectic mixtures. Thermal energy storage types made with phase change materials are sensible and latent heat storage.

Latent heat storage systems (LHSS) are leading the way in providing environmentally friendly energy saving solutions. Solid-liquid phase change materials are particularly attractive and innovative for thermal energy storage because they offer a wide temperature range between the four possible phase transitions in LHSS (solid-liquid, liquid-liquid, liquid-gas, solid-gas and solid-solid) and have high heat storage capacities. These systems are classified into 3 categories: organic, inorganic and eutectic types, as seen in the Figure 1, which heat storage during the transition from solid to liquid phase and release it during the transition from liquid to solid phase [1].

Thermal processes such as melting and solidification can be carried out with the help of infrared lamps. There are very few literature studies on these high current solar simulators. In the study conducted by Gallo et al., it is stated that solar simulators are widely used in cases where solar rays are not sufficient. In addition, solar simulators represent artificial high-current light sources similar to concentrated solar rays [2]. In a Similar literature study, a high flux solar simulator was used to provide process heat for glass production using concentrated solar radiation. Preliminary information on the use and applicability of concentrated solar radiation to melt glass at optimum scale was presented [3].

In the study conducted by Sarı and Karaipekli, in order to obtain a stable composite as a phase change material (PCM), the determination of the appropriate amount of paraffin (n-docosane) absorbed into Expanded Graphite (EG) and the effect of EG addition on thermal conductivity were investigated using the transient hot wire method. The thermal conductivity of pure paraffin and composite PCMs containing 2%, 4%, 7%, and 10% EG by weight was measured as 0.22, 0.40, 0.52, 0.68, and 0.82 W/mK, respectively. For these composite PCMs, the composite containing 10% EG is more suitable for latent heat storage with higher thermal conductivity and better melting temperature [4].

In the study by Akgün et al., a vertical tube geometry was designed to determine the charging and discharging properties of paraffin as a phase change material. The thermophysical properties of the investigated paraffin were determined by differential scanning calorimetry analysis. The effect of increasing the inlet temperature and mass flow rate of the heat transfer fluid (HTA) on both the charging and discharging

Corresponding Author: Ali Kemal Özcan
E-mail: ozcants61@gmail.com

How to cite this article:

Özcan, A.K., Öksüz, Ö., Demirtaş C., Experimental and numerical investigation of the use of organic and inorganic materials melted with infrared rays for thermal energy storage, The International Journal of Materials and Engineering Technology (TIJMET), 2024, 7(2): 85-99

processes of the PCM was investigated. An increase in the inlet temperature of the heat transfer fluid resulted in shorter melting times [5].

In order to increase the thermal conductivity of paraffin, the melting processes of pure paraffin and paraffin with 10% Al_2O_3 nanoparticle doping by mass in a two-dimensional rectangular melting area were investigated numerically with ANSYS Fluent software by Arslan et al. The effect of increasing the wall temperature of the rectangular area to 65 °C, 70 °C and 75 °C on the total melting time for pure paraffin and nanoparticle-doped paraffin was investigated. As a result, it was found that the use of Al_2O_3 nanoparticles increased the heat transfer rate of paraffin [6].

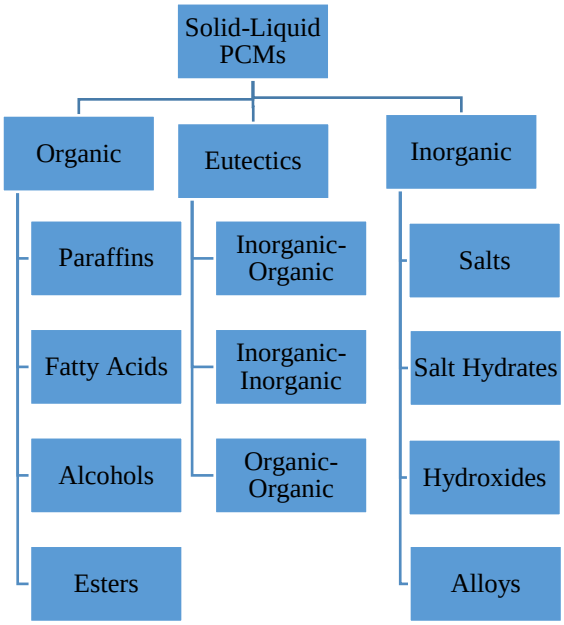

Figure 1. Classification of PCMs [1]

By Sinaringati et al., Paraffin and beeswax were used as PCM that can give off heat energy to heat the baby incubator. Paraffin and wax have high latent heat to keep the heat at constant temperature and release it. As a result, the PCMs were able to maintain heat energy at a temperature above 305 K for more than 8 hours in the infant incubator room. However, it was observed that beeswax performed better than paraffin in thermal energy storage [7].

There are many studies on molten salts. In this literature study, various triple and quadruple salt formulations containing NO_3/NO_2 as an anion in addition to lithium and calcium in their formulations have been investigated in order to lower the melting points of molten salts for heat storage and thus provide higher operating temperature ranges [8]. By Fernandez et al., in order to improve the current solar salt used as thermal energy storage fluid in Concentrated Solar Power plants, Hitec blend consisting of 53% KNO_3, 40% $NaNO_2$ and 7% $NaNO_3$ by mass has been extensively studied. The Hitec molten salt shows better physicochemical properties than the binary solar salt (60% $NaNO_3$ 40% KNO_3) due to its lower melting point, which can improve the operating temperature range in commercial solar power plants [9].

By Chauhan et al., solar dryers integrated with thermal energy storage units using paraffin wax were comprehensively investigated. Different types of paraffin wax and their thermophysical properties were presented, the thermal performances of solar dryer with paraffin wax and without paraffin wax were investigated and their effects on drying time and drying efficiency were reported. Furthermore, different locations of TES units in the dryer were reviewed and methods to increase the heat transfer rate between paraffin wax and drying air were investigated. The advantages and challenges of using paraffin wax in solar drying technology were also discussed [10].

A study conducted by Kraiem et al., at the CERTES laboratory of Paris Est University, focusing on the thermophysical characterization of four paraffin's (RT21, RT27, RT35HC, RT50) at different temperatures in both solid and liquid phases showed that melting temperatures and latent heats decreased with increasing heating rate. The study observed that the thermal conductivity increases with temperature in the solid phase but decreases with increasing temperature in the liquid phase. It was also found that thermal diffusions in the liquid state decreased with temperature [1].

The rays coming out of the infrared lamp are aimed to be focused on the determined area by conical reflector. The originality of this study lies in the numerical and experimental investigation of the use of organic phase change material (paraffin) and inorganic phase change material (Hitec salt) molten using concentrated infrared rays in thermal energy storage. Both materials are analyzed for their potential in sensible and latent heat storage across medium to high temperature applications, ranging from 100 °C to 300 °C. In this study, the heat flux entering the furnace is found theoretically by determining the absorption coefficient and emissivity rate of the energy coming to the furnace by the PCM and finding the heat flux at the focus. Thus, the first law of thermodynamics efficiency of this system is also calculated. In this study, where the Computational Fluid Dynamics (CFD) finite element method is used, ANSYS Fluent software is used to analyze the thermal behavior in the furnace. As a result of numerical and experimental data, it has been shown that charged PCMs can be used for up to approximately 4 hours. In addition, with this method, it is aimed to measure the amount of molten material (kg s^{-1}) depending on the infrared lamp power. Another aim is to present the stored thermal energy to the areas where it will be used, through heat exchangers created inside or outside the furnace. By performing processes without contacting organic and inorganic materials with the thermal power created by the rays, the harmful effects especially caused by the electrical conductivity of inorganic materials were also eliminated. In cases where renewable energy sources such as solar energy are insufficient, fuel heaters, infrared heaters and resistance heaters can be used as alternatives to provide continuous and reliable power.

2. Materials and methods

Infrared lamps, which are used artificially as substitutes for sunlight, are known for emitting both light and heat. The rays from the infrared lamp are focused on the furnace through a conical concentrator. Infrared lamps with different power ratings can be used depending on the desired focal temperature in the furnace. In this study, a single 500 W Golden Fer brand infrared lamp, powered by 220 V, was used. Additionally, the infrared lamp can be adjusted vertically to maintain a constant focal temperature. The infrared rays focused on the furnace melt the organic or inorganic phase change materials (PCMs), enabling thermal energy storage using materials with high heat capacity.

2.1. Experimental setup of the infrared lamp concentrator system

The infrared lamp concentrator system is based on the principle of focusing artificial rays onto a single point. A concentrator is placed between the light source and the receiver. The schematic representation of the ideal reflection of the infrared lamp and the basic geometric parameters of the conical concentrator system are shown in Figure 2. The number of conical concentrators can be increased up to the limit defined by the receiver surface area. Accordingly, the number of infrared lamps used corresponds to the number of conical concentrators. The physical properties and geometric dimensions of the conical concentrator system with the infrared lamp are provided in Table 1.

In the in Figure 2, A simple setup related to the reflection of the infrared ray concentrator system has been presented. Additionally, the infrared lamp is positioned at a 90° angle to the upper platform, which is designed to move up and down for adjustment if necessary. The infrared lamp and the concentrator can move together. This allows the artificial ray concentrator system to be easily positioned in the focal area of the receiving furnace. T-type thermocouples are placed at the bottom, middle, and top of the furnace to take temperature measurements. For the experiments, a 12-channel Lutron-brand datalogger with K-type and T-type thermocouples is used. Additionally, a K-type thermocouple is placed in the furnace for focal point temperature measurement. Temperature measurements are also taken with a thermal camera to support the thermocouple readings. The Fluke TiX501 thermal camera is capable of measuring temperatures in the range of -20 °C to 650 °C, with a thermal sensitivity of 0.075 °C at 30 °C and an infrared spectrum band of 7.5 µm to 14 µm.

2.2. Heat storage experiment of paraffin melted with infrared lamp

In the first experiment, paraffin (C_nH_{2n+2}) suitable for low-temperature applications, was used as the PCM. The thermophysical properties of the paraffin used for thermal energy storage are provided in Table 2 [11]. A 9-liter glass jar was utilized as the furnace, with the surroundings insulated using glass wool and aluminum foil. The use of a glass furnace enables observation and measurement of the melted paraffin. A total of nine T-type thermocouples were placed in the jar furnace at the bottom, middle, and top, while two K-type thermocouples were positioned in the focal region. A schematic and general view of the paraffin experimental setup is presented in Figure 3. The paraffin was melted and poured into the glass furnace to ensure homogeneous distribution. Once the paraffin cooled and solidified in the furnace, experiments were conducted using the ray concentrator system.

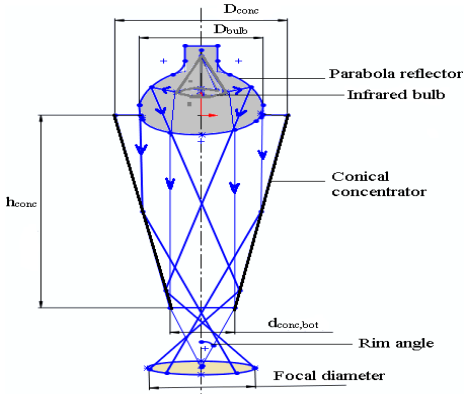

Figure 2. Schematic view of the positioning and geometric dimensions of the conical concentrator and infrared lamp

Table 1. Geometric properties and dimensions of the conical concentrator with infrared lamp

Geometric properties	Symbol	Value
Infrared lamp diameter	D_{lamp}	12 cm
Conical concentrator top diameter	D_{conc}	16 cm
Conical concentrator bottom diameter	$d_{conc,bot}$	6 cm
Conical concentrator length	h_{conc}	25 cm
Receiver focal diameter	d_{focal}	8 cm
Rim angle of concentrator	φ_R	22.6°

Table 2. Thermophysical properties of paraffin [11]

Parameters	Symbol	Value
Density (kg m^{-3})	P	870 (T= 300K) 780 (T= 340K)
Specific heat c_p (J kg^{-1}K^{-1})	c_p	2900
Thermal conductivity coefficient (W m^{-1}K^{-1})	K	0.24 (T=300K) 0.22 (T= 340K)
Viscosity (kg m^{-1}s^{-1})	µ	0.0057933
Latent heat of fusion (kJ kg^{-1})	L_e	190
Melting temperature (K)	T_m	331
Evaporation temperature (K)	T_b	355

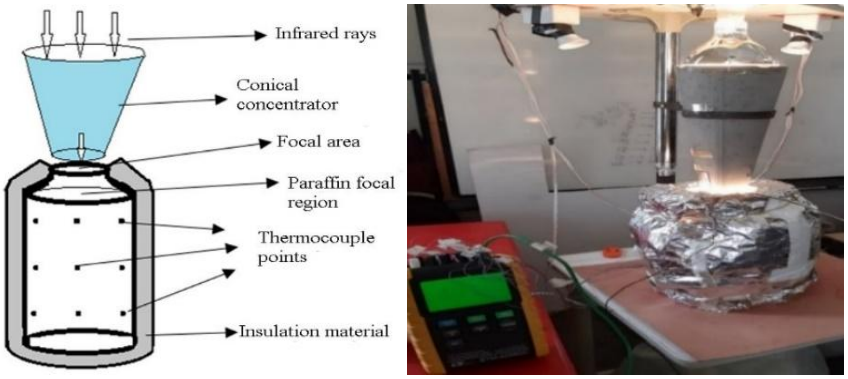

Figure 3. Schematic view of paraffin heat storage with infrared lamp and its appearance in the experiment

In the experiments, the temperature of the ray concentrator was initially adjusted due to the low evaporation point of paraffin (355 K). The temperature achieved by the rays entering the furnace was maintained at approximately 80 °C. Consequently, while the upper region of the paraffin in the furnace reached a temperature of about 80 °C, the temperature

gradually decreased toward the bottom of the furnace. In Figure 4, a thermal camera (TiX501) image shows a temperature of 73.29 °C near the top of the furnace and 24.55 °C at the bottom. Meanwhile, the temperature measured at the conical concentrator was 128.81 °C

When Figure 5 is examined, the temperature of the upper region, measured with a thermal camera by momentarily opening the glass vertically from the edge of the furnace, is 74.4 °C, while the temperature near the middle region is 24.66 °C. Additionally, the emissivity coefficient measured by the thermal camera in these regions is 0.95.

2.3. Heat storage experiment of Hitec salt melted with infrared lamp

Inorganic Hitec salt (53% KNO_3, 40% $NaNO_2$, and 7% $NaNO_3$), with a low melting point and high heat storage capacity, was used as a PCM in conjunction with the ray concentrator system. The thermophysical properties of the Hitec salt used for heat storage are provided in Table 3 [12,13]. To prepare approximately 26 kg of Hitec salt, 53% potassium nitrate, 40% sodium nitrite, and 7% sodium nitrate were mixed by weight and melted in an electric furnace. To homogenize the Hitec salt to 99% purity, it was cooled and ground into a powder. The powdered Hitec salt was then poured into the furnace. After preparation, the Hitec salt was calibrated by verifying its suitability for the desired melting temperature. A general view and schematic of the prepared Hitec salt heat storage experiment are shown in Figure 6. A 10-liter stainless steel furnace was used, with six T-type thermocouples placed at the bottom, middle, and top points, and two K-type thermocouples placed in the focal region. The top of the furnace was covered with quartz glass to allow the passage of rays. The difference in this experiment was that all the rays were allowed to enter the furnace. As a result, high temperatures were achieved inside the furnace, causing the Hitec salt to begin melting.

Figure 4. An image of the infrared lamp experimental level taken with a thermal camera

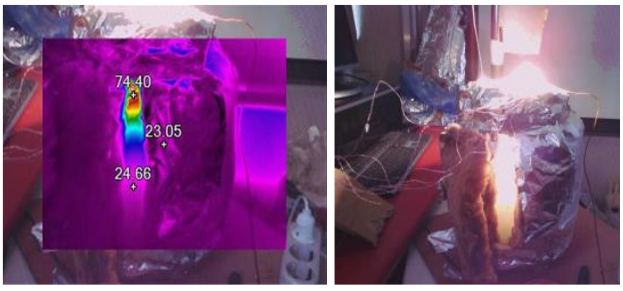

Figure 5. Images taken with a thermal camera over the glass furnace in the paraffin experiment

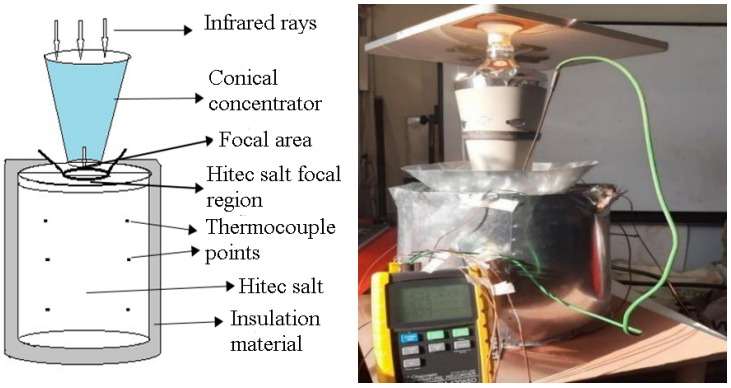

Figure 6. Schematic view of heat storage of Hitec salt by infrared lamp and its image in the experiment

Table 3. Some physical properties of Hitec salt [12,13]

Parameters	Symbol	Value
Density (solid-liquid)	ρ	(2013-1857) kg m^{-3}
Specific heat (solid-liquid)	c_p	(1090-1570) J kg^{-1} K^{-1}
Thermal conductivity coefficient (solid-liquid)	k	(0.74-0.439) W m^{-1} K^{-1}
Latent heat of fusion	L_e	83740 J kg^{-1}
Viscosity	μ	(0.024-0.0012) kg m^{-1} s^{-1}
Melting point temperature	T_m	415 K
Stable max operating temperature	T_b	811 K

2.4. Thermal energy conversion calculations in furnace with infrared rays

Thermal storage is achieved through the latent and sensible heat absorbed during the melting of these substances. The thermal energy storage system is typically analyzed in three stages: energy loading (charging), energy storage, and energy discharge, as shown in Figure 7. When the furnace is considered as a closed system, the differences in energy entering and leaving the furnace are balanced by the sensible and latent heat stored within the furnace. It is assumed that no work is performed within the system and that there are no changes in kinetic or potential energy. The energy balance for the furnace

is given by Eq. (1) [14]. The amount of energy stored in the furnace is calculated by Eq. (2) [14-17].

$$\frac{d(m\,c_p T+mL)}{dt} = E_{fur,in} - E_{fur,out} \quad (1)$$

$$\Delta E = \dot{m}_l\,\beta\,c_p(T_l - T_a) + \dot{m}_l\,L + \dot{m}_s\,(1-\beta)\,c_p(T_s - T_a) \quad (2)$$

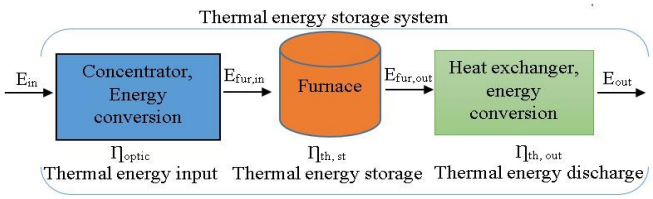

Figure 7. Energy balance status of the thermal energy storage system

For the charging state, the efficiency of the furnace, according to the first law of Thermodynamics, is calculated as the ratio of the energy stored in the furnace to the energy entering the furnace, as shown in Eq. (3) [18].

$$\eta_{th,st} = \frac{E_{st}}{E_{fur,in}} = \frac{\dot{m}_l\,\beta\,c_p(T_l - T_a) + \dot{m}_s\,L + \dot{m}_s(1-\beta)\,c_p\,(T_s - T_a)}{I\,A\,\eta_{op}} \quad (3)$$

Where T_l (K) is the average temperature of the molten liquid state of the substance in the furnace, T_s (K) is the average temperature of the solid state of the substance in the furnace, T_a (K) is the ambient temperature, β is the liquid fraction of the molten substance, $\dot{m}_l$ (kg/s) is the mass flow rate of the molten substance in the liquid state, $\dot{m}_s$(kg/s) is mass flow rate of the substance remaining from melting and E_{in} (W) is the amount of thermal energy entering the furnace. In order to find the energy entering the furnace, the heat flux of the infrared lamp to the concentrator was found. In order to find the heat flux, using the experimentally measured focal temperature values, the radiation value I (W/m^2) coming to the receiver was calculated with Eq. (4) by using the heat transfer equation with radiation [19-21].

$$I = \frac{\varepsilon\,\sigma}{\eta_{op}\times C_R\times\alpha\times\tau} \times \left(\frac{T_{focal}}{F_B R_S}\right)^4 \quad (4)$$

The optical efficiency η_{op} is calculated as 83.2% with Eq. (5) based on the reflective surface coefficient (0.9) and rim angle (22.6°) of the conical concentrator [20,25]. Where, the focal temperature was used within the degradation factor (F_B = 0.9) and cooling coefficient (R_S = 0.8) range to be closer to reality, as a result of an experimental study [20].

$$\eta_{op} = \cos\theta i \times \rho_{ref} \times (f_s\,\Gamma) \quad (5)$$

Where, θi is the incident ray angle, assuming that there is no cosine loss θi=0 are taken, ρ_{ref} concentrator reflective surface coefficient is taken as 0.9, and the shading and intercept factor is calculated by Eq. (6) [20,25].

$$f_s\Gamma = \frac{\sin^2\theta_R - \sin^2\theta_{min}}{4\tan^2(\frac{\theta_R}{2})} \quad (6)$$

Also, the shadow angle (θ_{min}) is taken as zero assuming that there is no shadow at the focus and. The concentrator rim angle was found to be θ_R = 22.6° as seen in Table 1. The geometric concentration ratio (C_R=A_c/A_r) is calculated as approximately 6.11. The permeability coefficient (τ) is taken as 0.92 for quartz glass through authorized companies.

The absorption coefficient of paraffin in the furnace with a penetration distance of 30 cm was found to be 0.6 [26]. As the thickness of the paraffin sample increases, its absorption coefficient increases and its permeability decreases. Using the emissivity model proposed by Astarita and Carlomagno [27] and a refractive index of 1.43 presented by Mark and Kroschwitz [28], a wall emissivity of 0.91 was found for paraffin wax [29, 30]. Table 4 shows the emissivity and absorption coefficient ranges of paraffin and Hitec salt. The emissivity of Hitec salt varies in the range of 0.6-0.8 for the melt temperatures between 150 and 400 °C and wavelengths between 500 and 1000 nanometers [31]. Hitec salt has a spectral absorption coefficient of 160-220 (m^{-1}) in the wavelength range of 500-1000 nanometers at the melt temperature of 150-400 C. This value shows that hitec salt has a very high absorption coefficient (α=0.95) in the liquid state [31].

Table 4. The emissivity and absorption coefficient ranges of paraffin and Hitec salt [26-31]

Materials	Emissivity, ε	Absorption coefficient, α
Paraffin	(0.91-0.95)	0.6±0.05
Hitec salt	(0.6-0.8)	0.9±0.05

2.5. Numerical CFD calculation

In the numerical method, the melting states and temperature values of the materials in the furnace were determined using ANSYS Fluent program. ANSYS Fluent is a CFD software using the finite volume method. Initially, the PCMs are in a solid state, with the PCM's starting temperature set at 300 K. The assumptions made during numerical modelling are as follows:

1- 2D state is considered as transient regimes.
2- The motion of PCMs in liquid state is incompressible, Newtonian and the flow is laminar.
3- While the viscosity of PCM varies, its density and thermal conductivity are assumed to change linearly.
4- Viscous heating and volume expansion are neglected.
5- PCM is considered isentropic and homogeneous.

Accordingly, continuity with Eq. (7), energy with Eq. (8), momentum with Eq. (9) for two dimensional transient laminar flow are given below [32, 33]. Continuity:

$$\frac{\partial\rho_f}{\partial t} + \nabla(\rho_f\overrightarrow{U}) = 0 \quad (7)$$

Energy:

$$\frac{\partial\,(\rho_f H)}{\partial t} + \nabla.\left(\rho_f\vec{U}H\right) = \nabla.(k_f\nabla T) \quad (8)$$

Momentum:

$$\frac{\rho}{\varepsilon}\frac{\partial u}{\partial t} + \frac{\rho_f}{\varepsilon^2}\left(\vec{U}\,\nabla u\right) = -\frac{\partial p}{\partial x} + \frac{\mu_f}{\varepsilon}\nabla^2 u + Su \quad (9)$$

$$\frac{\rho}{\varepsilon}\frac{\partial v}{\partial t} + \frac{\rho_f}{\varepsilon^2}\left(\vec{U}\,\nabla v\right) = -\frac{\partial p}{\partial y} + \frac{\mu_f}{\varepsilon}\nabla^2 v + \rho_f g\beta_{te}(T - T_m) + Sv \quad (10)$$

In the above conservation equations, $\vec{U}$ is the fluid velocity, ρ_f is the density, μ is the dynamics viscosity, P is the pressure, g is the gravitational acceleration, k is the thermal conductivity, β_{te} is the coefficient of thermal expansion. In addition, H is the

total enthalpy of the molten material and is calculated as the sum of sensible enthalpy and latent heat as follows.

$$H = h + \Delta H = h_{ref} + \int_{T_{ref}}^{T} c_p \, dT + \beta L_{sf} \quad (11)$$

β for the melt liquid fraction is defined as follows [32, 34, 35].

- If $T<T_S$, $\beta=0$. If $T>T_l$, $\beta=1$.
- If $T_s<T<T_l$ at the interface $\beta = \frac{T-T_s}{T_l-T_s}$

The momentum loss due to decreasing porosity in the partially solid region was calculated with Eq. (12) [32, 35]

$$S = \frac{(1-\beta)^2}{(\beta^3-\varepsilon)} A_{mush}(\vec{U}) \quad (12)$$

Here $\dot{\varepsilon}$ is a very small number (0.001) to avoid division by zero [35] and the coefficient A_{mush} is a mushy zone constant which is fixed at a value of 10^5 kg $m^{-3}s$ [32].

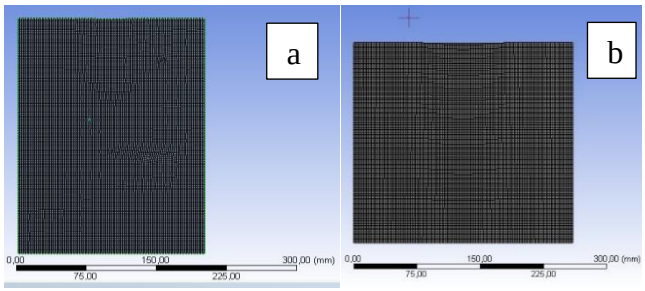

Figure 8. 2D mesh structures of the relevant furnaces; a) paraffin and b) Hitec salt

2.5.1. Numerical CFD calculation of furnace filled with paraffin

First, the initial and boundary conditions were determined for the paraffin solution in the Fluent program. In accordance with the experimental conditions, the mesh structure of the furnace filled with paraffin, with dimensions of 20x28 cm, is shown in Fig. 8a. Due to the large number of elements and nodes in the furnace model and the lengthy computation time required for numerical analysis (which depends on the computer's processing speed), faster results were obtained by designing a 2D model. The element size for paraffin in this model is 2 mm, with 14,278 nodes and 14,039 elements. The mesh structure was created as uniform in CFD Fluent to achieve more realistic results based on element size. For the boundary conditions of the model, the focal surface temperature was set to 100 °C, and all other surfaces were assumed to be insulated (q" = 0). In this model, the flow was assumed to be laminar with a low velocity. The coupling between pressure and velocity was solved using the SIMPLE algorithm, with pressure-velocity fields, momentum, and continuity equations. For pressure interpolation, the PRESTO method was chosen, as it is suitable for any mesh structure. The energy and momentum equations were solved using second-order upwind, and the transient formulation equations were set to second order. For paraffin, the optimal time step was 0.3 s, and the number of iterations was set to 25 to achieve stable temperatures and increasing melting rates.

2.5.2. Numerical CFD calculation of furnace filled with Hitec salt

The mesh structures of the furnace filled with Hitec salt with dimensions of 26x26 cm are given in Figure 8b. This furnace has a mesh structure with an element size of 2 mm, number of nodes 16,632 and number of elements 16,375, and a skewness value of 0.9. In the transient regime, energy, solidification and melting equations were selected in the modelling. Hitec salt was chosen as the fluid material and the focal point was assumed to be 200 °C and the other surfaces were insulated with 1 mm steel material depending on the experimental conditions as the boundary condition. This Hitec furnace model was numerically analysed similar to paraffin. In this model, the viscous flow was chosen to be laminar with low velocity assumption. The coupling between pressure and velocity using the pressure and velocity fields, momentum and continuity equations is solved with the SIMPLE algorithm. For pressure interpolation, PRESTO was chosen. The energy and momentum equations are second order upwind and the transient formulation equations are second order. For Hitec salt, the optimal time step was 0.3 s and the number of iterations was 25.

2.6. Uncertainty analysis of heat storage system with infrared ray

Uncertainty analysis is performed due to measurement errors and assumption errors made for numerical and experimental thermal analysis. Some error values of this system; Error due to thermocouple pairs ± 0.75 °C, Average error due to digital thermometer ± 0.5 °C, Average error in furnace interior temperature measurement ± 3°C, Surface reflection angle 2%, Incident beam angle 2% and Incident light power error 5%. According to these data, the total uncertainty ratio of the infrared ray concentrator system is calculated as approximately 6.5% with the uncertainty equation obtained by Kline and McClintock [36]. This uncertainty value is suitable for the experimental data.

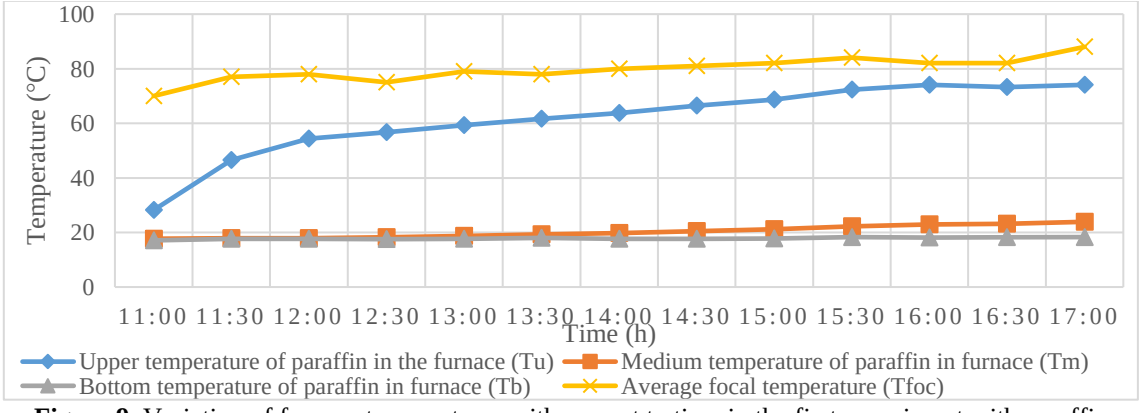

Figure 9. Variation of furnace temperatures with respect to time in the first experiment with paraffin

3. Results

The differences and similarities of paraffin and Hitec salt materials in thermal energy storage were investigated in the laboratory using experimental and numerical CFD methods and the results are presented.

3.1. Experimental data in laboratory environment

3.1.1. Experimental data on thermal energy storage with paraffin

The data obtained from the paraffin melting experiment with an infrared lamp, when the ambient temperature was between 17 °C and 19 °C, are presented graphically in Figure 9. In the 28 cm high furnace, it can be observed that the temperature in the upper region gradually approaches the focal temperature over time. As paraffin began to melt at approximately 60 °C, the temperature in the upper region increased. Due to the low thermal conductivity, the average temperature in the bottom region of the paraffin in the furnace remained around 19 °C. Approximately 0.7 kg of paraffin was melted over the 4-hour duration of the experiment. Based on this, the melting flow rate was calculated to be approximately 0.047 g s^{-1} using the 500 W infrared lamp power.

Table 5. Paraffin heat storage charging experiment data

Time	Upper temperature of paraffin T_u, (°C)	Middle temperature of paraffin T_m, (°C)	Bottom temperature of paraffin T_b, (°C)	Average focal temperature T_{foc}, (°C)	Paraffin focal surface temperature T_s, (°C)	Ambient temperature T_a, (°C)
11:00	30,2	17,8	17,75	170	76	18
11:30	38,45	18,1	17,95	200	79	18
12:00	48,45	18,3	18,05	220	82	19
12:30	60,9	18,8	18,15	211	81	19
13:00	68,3	19,35	18,15	213	83	19
13:30	73,1	20,05	18,35	210	83	19
14:00	77,2	20,8	18,5	213	80	19
14:30	77,8	21,5	18,55	210	80	19
15:00	78,6	22,1	18,65	210	80	19

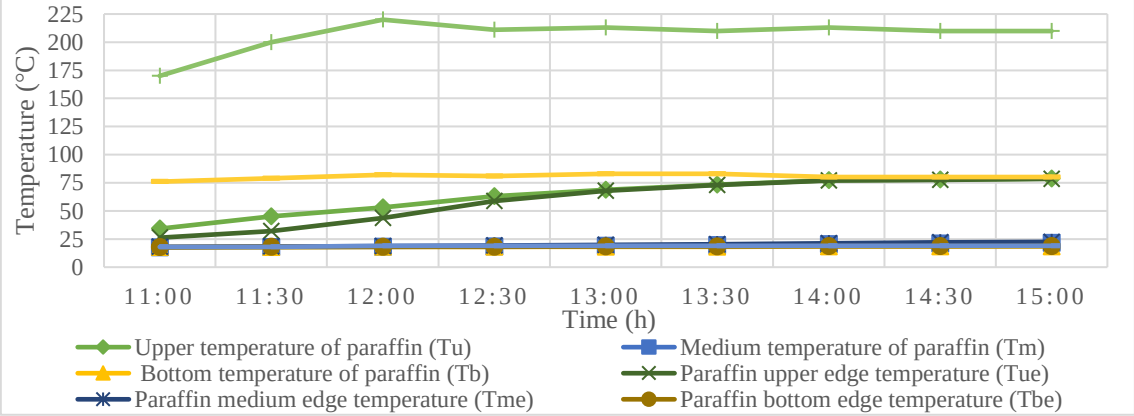

Figure 10. Furnace temperature curves of the second charging experiment with paraffin

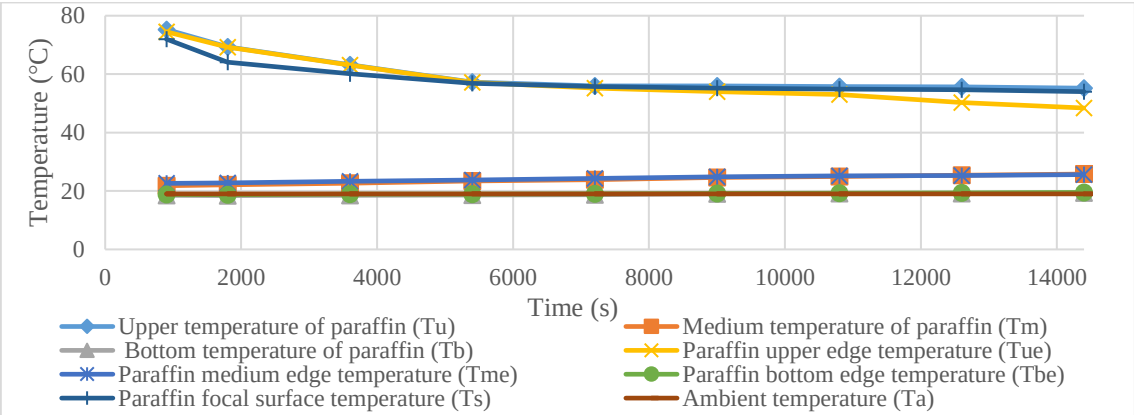

Figure 11. Temperature curves of the furnace depending on time in case of paraffin discharge

The paraffin thermal energy storage charging experiment is carried out by keeping the top surface temperature at approximately 80 °C considering the paraffin evaporation temperature as shown in Table 5. As seen in Figure 10, the average focal temperature is 210 °C, while higher temperatures are obtained in the upper region. Due to the low thermal

conductivity of paraffin, the temperature change in the bottom regions of the furnace is slow.

Figure 11 shows that in the case of paraffin discharge, the upper region temperature is 75 °C and dropped to approximately 55 °C after 4 hours. In the bottom regions of the furnace, a slight increase continues, indicating that the stored energy can be used for at least 6 hours.

3.2. Experimental data on thermal energy storage with Hitec salt

The infrared lamp used had a power of 500 W, and the infrared rays were concentrated in a focal surface area of about 8 cm using a conical concentrator. In the experiment, conducted at an ambient temperature of 20 °C, it was observed that the Hitec salt began to melt in approximately 10 minutes. Additionally, reflection losses between the infrared lamp and the conical concentrator were reduced in this experiment. The average data obtained from the thermal energy storage experiment using the infrared lamp are presented in Table 6. Furthermore, Figure 12 illustrates the graph showing the variation of the focal and furnace temperatures over time during the infrared lamp experiment. The focal temperature varied between approximately 280 °C and 300 °C, while an average temperature of 220 °C was observed on the upper surface of the furnace during the charging process. After 4 hours, the temperature in the upper region of the furnace reached 116 °C. Meanwhile, the temperature of the Hitec salt in the middle region of the furnace increased over time, with the highest temperature measured at 87 °C. The rate of temperature increase in the middle region was lower compared to the measurements taken at the bottom of the furnace, where the highest temperature measured was 39 °C.

In these experiments, the furnaces were insulated with glass wool and only the upper region had an opening through which the rays entered. In the second experiment with Hitec salt, the focal area was covered with a quartz glass to reduce the loss of natural convection in the furnace.

In the discharge state, measurements were continued when the infrared lamp charging experiment was completed. The temperature values measured for two hours are given in Table 7. In addition, in the discharge condition, Figure 13 shows the furnace internal temperature change graph according to time. According to this, Hitec salt temperatures remained approximately constant in the botom region of the furnace for two hours. The temperature in the middle region of the furnace, which is 86°C at the beginning, decreased by 65% to 56°C after two hours. The temperature of the upper region inside the furnace is observed to decrease more rapidly due to the heat loss from the furnace open to the atmosphere.

At the end of the discharge phase, it was observed that the average temperature of the upper region of the Hitec salt in the furnace dropped from approximately 102 °C to 46 °C. Thus, it has been revealed that with the current size of Hitec salt, the stored thermal energy can be transferred to the usage area for at least 4 hours.

Table 6. Data obtained from Hitec salt experiment with infared lamp

Time (s)	Focal temperature (°C)	Focal temperature in the furnace (°C)	Upper temperature of Hitec salt in the furnace (°C)	Middle temperature of Hitec salt in the furnace (°C)	Bottom temperature of Hitec salt in the furnace (°C)
1800	316	210	49	36	22
3600	300	212	72	45	23
5400	290	218	80	56	24
7200	290	240	85	64	27
9000	280	230	95	69	29
10800	281	222	104	82	34
12600	280	219	112	86	34
14400	276	215	116	87	35

Table 7. Data obtained from the Infrared lamp experiment for the discharge state

Time (s)	Upper temperature of Hitec salt (°C)	Middle temperature of Hitec salt (°C)	Bottom left edge temperature of Hitec salt (°C)	Bottom right edge temperature of Hitec salt (°C)
900	102	86	28	37
1800	85	77	28	37
2700	75	72	28	38
3600	70	69	27	38
4500	63	64	27	38
5400	58	61	27	38
6300	57	58	27	37
7200	55	56	27	37

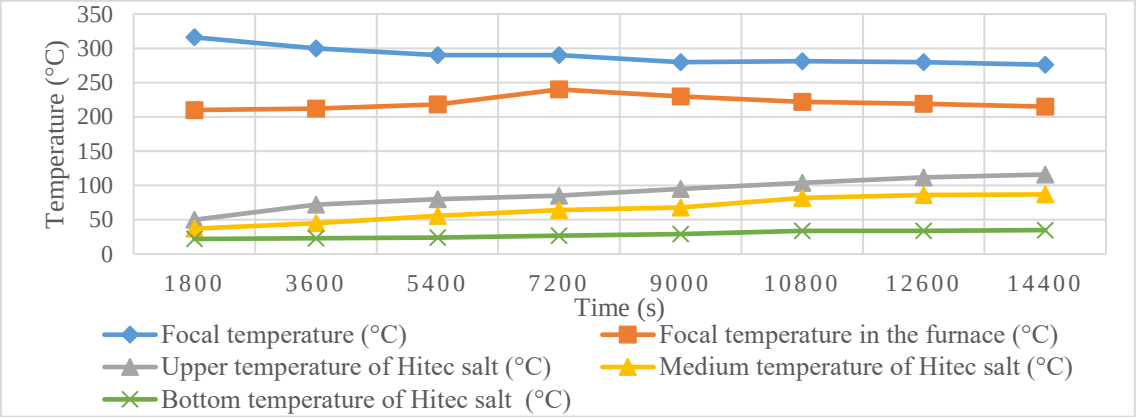

Figure 12. Variation of Hitec salt temperatures with time for the charging state of the furnace

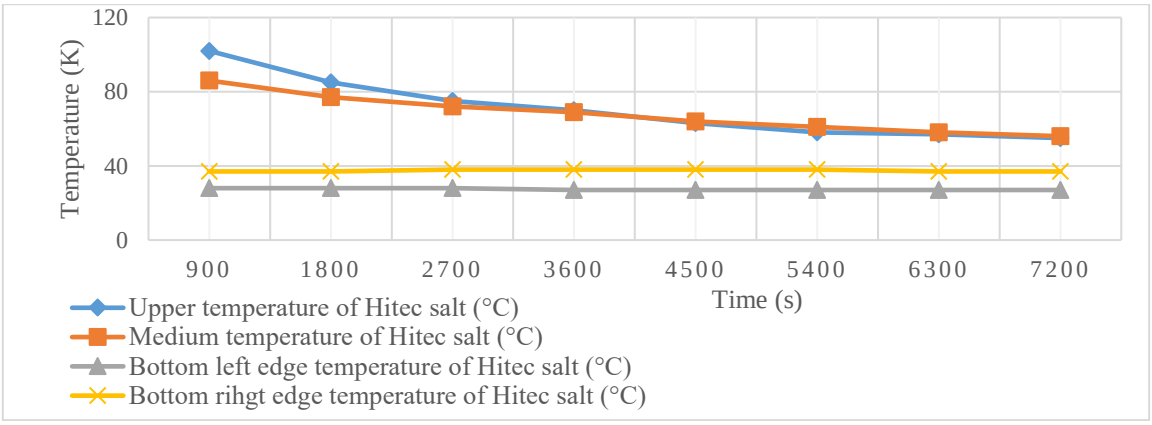

Figure 13. Temperature change of the furnace with Hitec salt according to time in the experiment conducted in discharge state

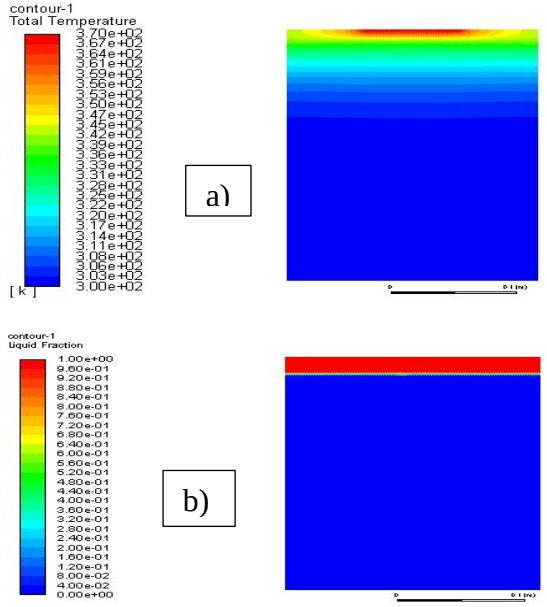

Figure 14. Contours of paraffin in the furnace in numerical analysis; a) temperature and b) melting

3.2. Numerical CFD results

Numerical CFD results for the melting and temperature conditions of paraffin and Hitec salt are given below.

3.2.1. Numerical CFD results for paraffin in storage furnace

The temperature and melting contours of the data obtained from numerical paraffin melting solidification modelling at the end of four hours are given in Figure 14. As seen in Figure 14a, while the focal temperatures are kept at the vaporization temperature of paraffin, the regions close to the focal point are at higher temperatures, while the temperature change at the bottom of the furnace is very small. In Figure 14b, the melting rate of paraffin is approximately 7% and the mass flow rate is calculated as 3.69×10^{-5} kg/s. Due to the low coefficient of conductivity of paraffin, heat transfer towards the furnace bottom was found to be slow.

3.2.2. Numerical CFD results for Hitec salt in the storage furnace

According to the data obtained in the numerical analysis with Hitec salt, the focal point temperature (475 K) is kept higher than paraffin for the melting of Hitec salt. The temperature contours of Hitec salt at the end of 6 hours in numerical analysis are given in Figure 17a and melting contours in Figure 17b. As seen in Figure 17a, the temperature in the middle region of the furnace is around 86°C, and the temperature in the upper region is around 116°C, which is in agreement with the experimental data. As can be seen in Figure 18, the average temperature of Hitec salt increases and the average temperature reached at the end of 4 hours is 328 K. The volumetric fraction of liquid melted increased with time, reaching 3.1% after 4 hours and approaching 6% after 6 hours as shown in Figure 19. Figure 15 also shows that the temperature of the entire paraffin in the furnace increased over time. Additionally, Figure 16 demonstrates that the liquid portion of the paraffin in the furnace, in the melting state, increased over time. It has been found that the temperature distribution and melting rates obtained experimentally are approximately similar to each other.

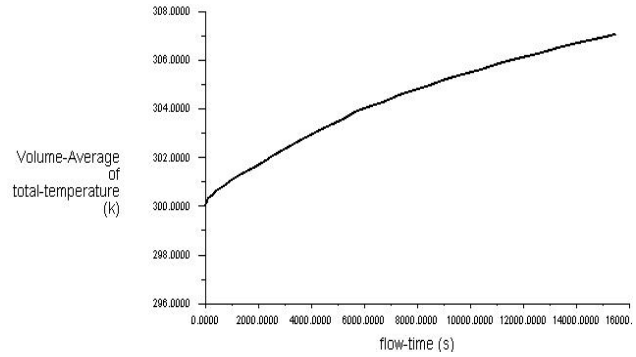

Figure 15. Variation of all paraffin temperature in the furnace with time

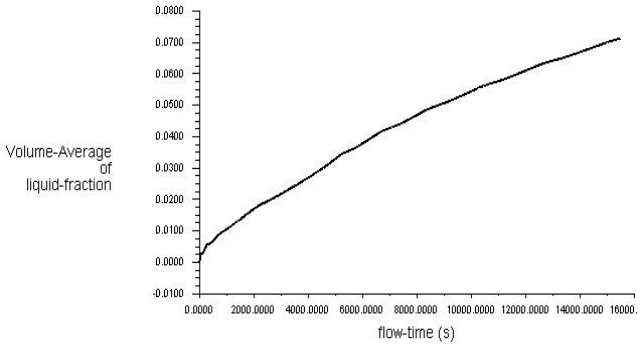

Figure 16. Variation of the liquid fraction (β) of paraffin in the furnace with time

4. Discussion

4.1. Verifying and comparing of paraffin and Hitec salt data

In the Figure 20 shows the variation of numerical and experimental data of paraffin with time. Accordingly, the temperature and melting rates obtained for paraffin are close to each other. In Figure 21 shows the variation of numerical and experimental data of Hitec salt with time. For Hitec salt, numerical and experimental data are shown parallel increases in the charge state.

The melting rates and mass flow rates obtained for paraffin and Hitec salt according to the data obtained according to experimental and numerical methods are given in Table 8. According to this table, while the melting rate was 8.9% in the furnace with 7.6 kg of paraffin, the melting rate was 3.4% in the furnace with 26 kg of Hitec salt. When compared in terms of mass flow rate, the mass flow rate of Hitec salt is higher than paraffin. At the end of 4 hours, the mass flow rates of PCMs in the furnace were determined as 0.047 g s^{-1} and 0.061 g s^{-1} for Paraffin and Hitec, respectively.

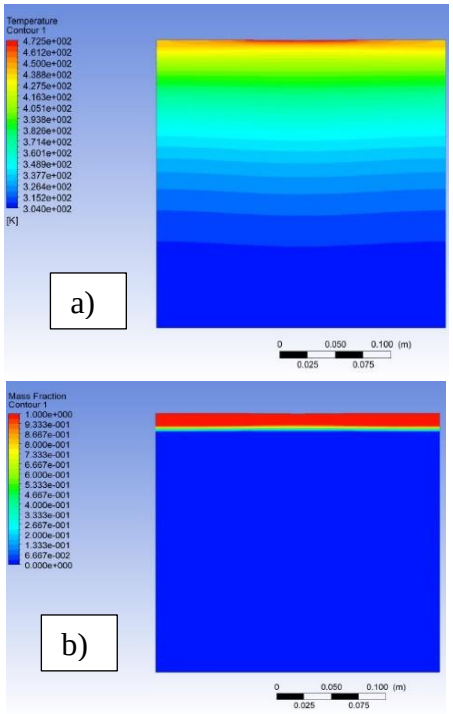

Figure 17. Contours of Hitec salt in the furnace numerically; a) Temperature and b) melting

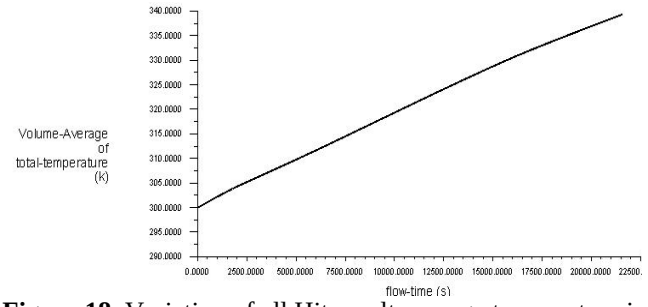

Figure 18. Variation of all Hitec salt average temperature in the furnace with time

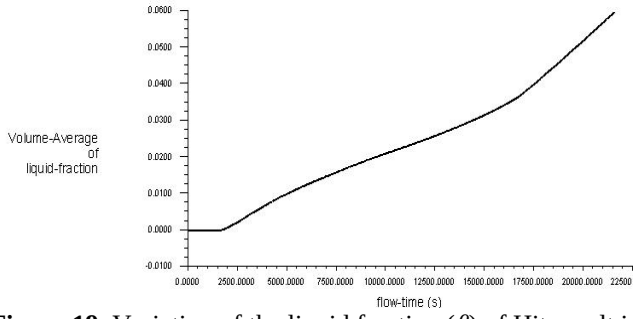

Figure 19. Variation of the liquid fraction (β) of Hitec salt in the furnace with time

Table 8. Melting flow rates and melting rates in the furnace for paraffin and Hitec salt

Method	Paraffin Melting ratio β (%)	Mass flow ratio $\dot{m}$ (g s^{-1})	Hitec Melting ratio β (%) salt	Mass flow ratio $\dot{m}$ (g s^{-1})
Experimental	8.9	0.047	3.4	0.061
Numerical	7	0.037	3.1	0.056

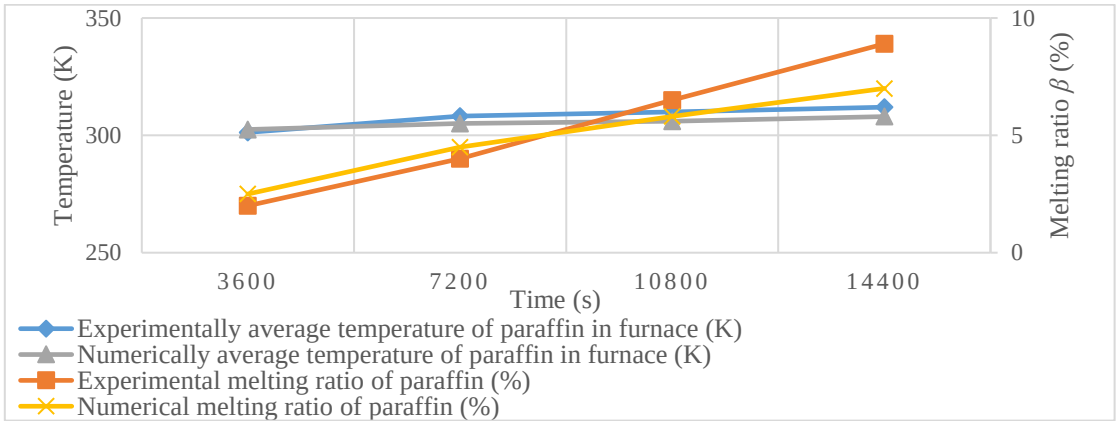

Figure 20. Comparison of numerical and experimental data for paraffin

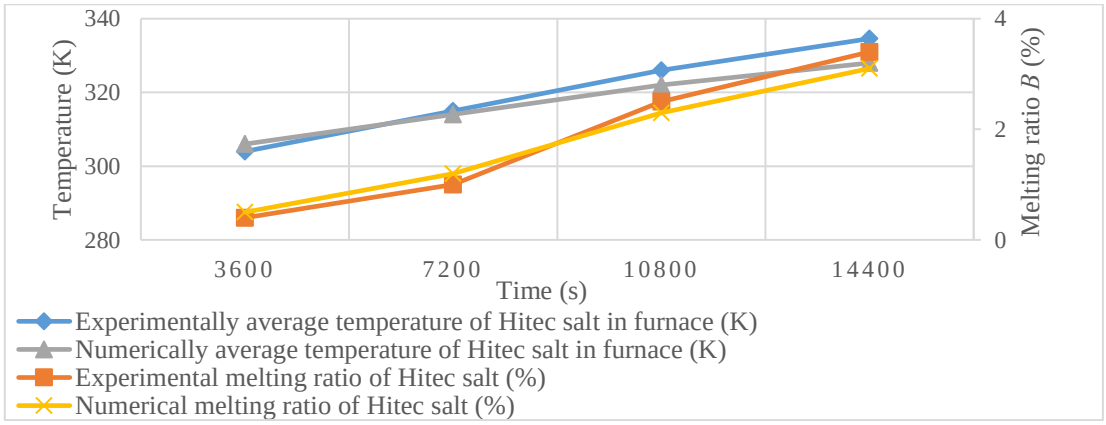

Figure 21. Comparison of numerical and experimental data for Hitec salt

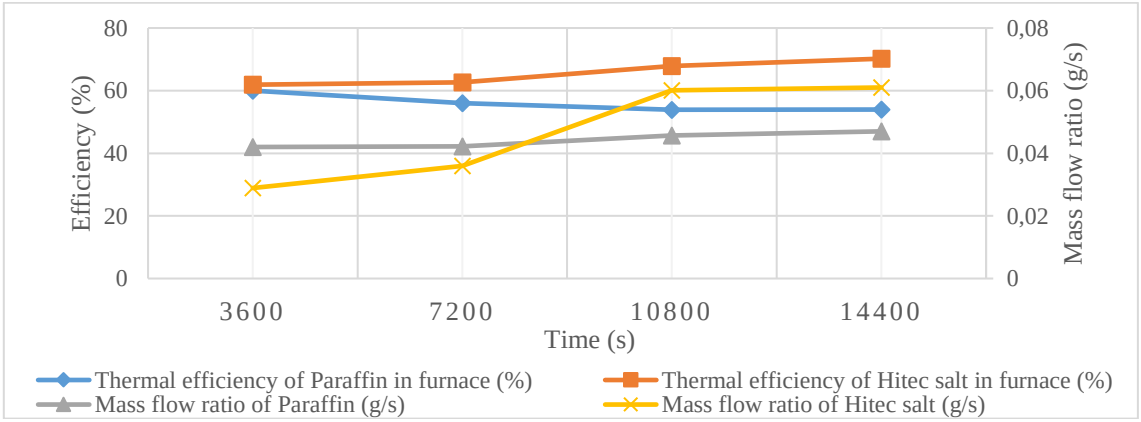

Figure 22. Thermal efficiency and mass flow rates of paraffin and Hitec salt in the furnace with time

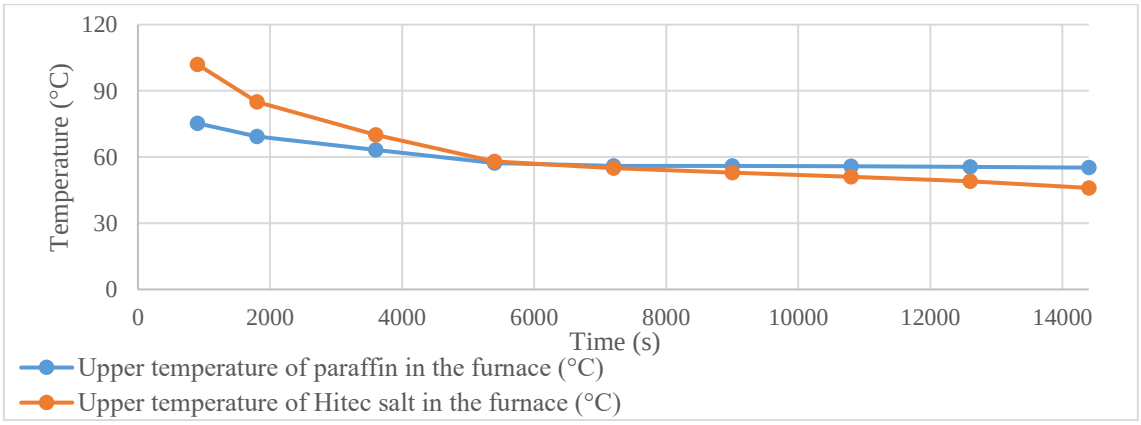

Figure 23. Time dependent temperature curve of Paraffin and Hitec salt for discharge condition

According to the focal temperatures measured in the experiments, the heat flux on the focal region of the furnace containing paraffin was calculated as 1218 W m^{-2}, while the heat flux on the focal region of the furnace containing Hitec salt was calculated as 1955 W m^{-2} with Eq. 4. Based on the experimental data with Eq. 4, the theoretically calculated heat fluxes of the infrared lamp were calculated as 3716 W m^{-2} for paraffin and 8447 W m^{-2} for Hitec. These heat fluxes were used in the thermal efficiency equations. The thermal efficiency and mass flow rates of paraffin and Hitec salt in the furnace varying with time are given in Figure 22. The average thermal efficiency of paraffin in the furnace was calculated to be approximately 56%, while the average thermal efficiency of Hitec salt in the furnace was calculated as 65.6%. Additionally, the first law of thermodynamics efficiency ($\eta_{total}=Q_{st}/Q_{in,\ electric}$) calculated for paraffin and Hitec salt are 8% and 19.7%, respectively. In this efficiency, 500 W electrical energy given to the system was used as the input energy.

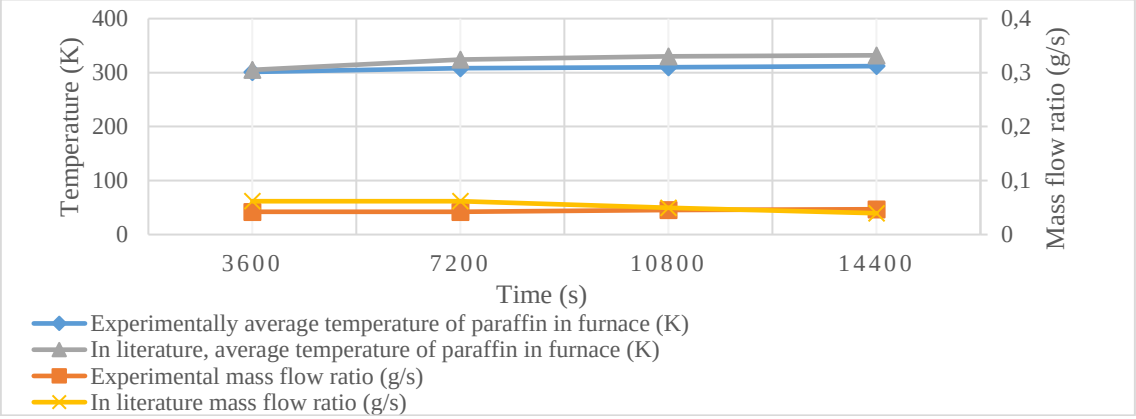

Figure 24. Comparison of this study with paraffin melting experiments of different sizes in the literature

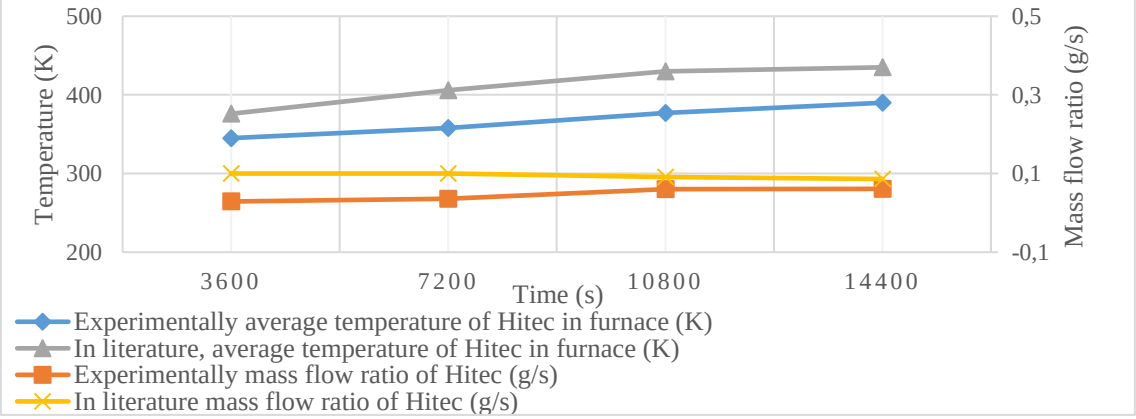

Figure 25. Comparison of similar literature on the melting of Hitec salt

According to the experimental results in the discharge, the graph of paraffin cooling at a slower rate than Hitec salt is given in Figure 23

4.2. Comparison of paraffin and Hitec salt with studies in the literature

The experimental data with paraffin in this study were compared with some studies in the literature by Ambarita et al. [23]. Accordingly, the temperature change graph of paraffin in the furnace obtained when heat input was made from different regions (side) and when a similar temperature (80 °C) input was made is given in Figure 24. It is seen that the melting flow rates obtained for 0.89 kg paraffin with dimensions of (10x10x10) mm in the literature and 7.6 kg paraffin in this study are close to each other. As in the literature, the melting flow rate is high at the beginning due to the heat given to the furnace from the side. In addition, the temperature difference is observed due to the low heat conduction coefficient according to the size difference of the furnaces.

The overall four tests confirmed that paraffin and beeswax have good ability to store heat energy at the temperature above 32 °C for over 8 hours in infant incubator [37]. In this study, it is revealed that the paraffin temperature varies between 60-80 C for 4 hours in the discharge state and is suitable for long-term heat storage.

In the literature, melting experiments conducted by Xiao et al. [24] on Hitec salt, heat transfer was made to furnaces of different sizes (cylindrical with a diameter of 95 mm and a length of 300 mm) from different surfaces. Despite these size differences, the literature study conducted with a temperature of 160 °C applied to an equal surface reached melting flow rates in the range (0.06-0.08) g s^{-1} similar to the study in this article, as seen in Figure 25. Considering the melting region in this study and the literature, there was little difference in Hitec salt temperatures since they have different surface areas and heat input surfaces. The study conducted by Xiao et al. on Hitec salt, for charging and discharging conditions, the furnace top temperature and middle temperatures in the experimental data in this article are compared in the graph in Figure 26 [24]. Accordingly, while the temperatures in the regions close to the heater are high, the temperatures in the regions approximately 5 cm away from the heater are lower. It is seen that the temperatures of the region 5 cm away from the heater (T6) are close to the furnace top and middle region temperatures in this

article. In the discharge condition, it is seen in Figure 26b that the T6 temperature point and the upper and middle temperatures have similar cooling curves.

Finally, if the infrared lamp simulators are compared, firstly, A radiation power of up to 2100 W with a maximum peak flux of 2700 kW m^{-2} was presented by Bellan et al. [38]. Secondly, by Kuhn and Hund, Using a 20 kW lamp, the simulator achieved a peak flux of approximately 16,000 kW m^{-2} and measured a radiation power of 3000 W inside a square with a side of 7 cm. Based on the lamp's electrical input, the conversion efficiency to radiation energy was 17% [39]. In this article, a heat flux of approximately 8500 W m^{-2} is achieved with a 500 W powerful infrared lamp, while the energy conversion efficiency is calculated as 19.7%. In addition, the focal heat flux can be increased by reducing reflection and optical losses in the focal area of approximately 8 cm.

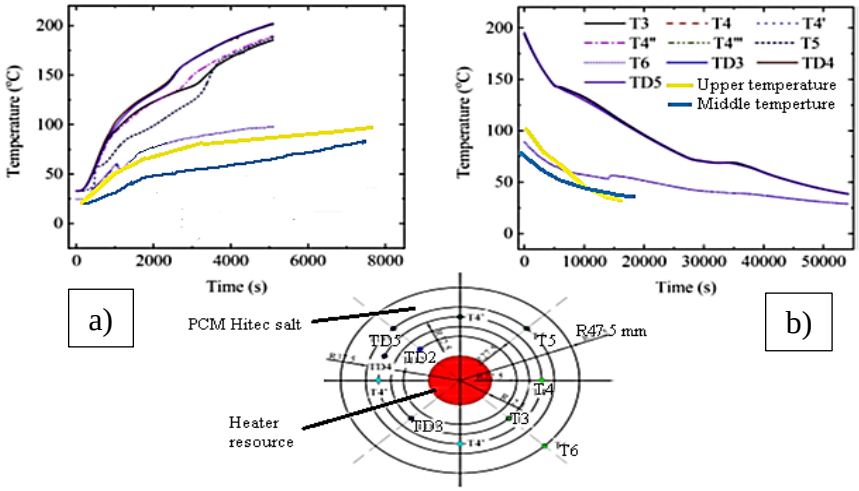

Figure 26. Temperature comparison with a study in the literature on Hitec salt a) in charge and b) in discharge [24]

4.3. Economic analysis of the system

The cost of the installed ray concentrator and heat storage system is quite low. The cost of all components of the system is listed in Table 9. The total installation cost was calculated to be $300. In addition to the installation cost, there is the electricity consumption of the infrared lamps. The infrared lamp power used for the designed ray concentrator system is 500 W. In this case, if the unit price of electricity in Turkey for 2024 is approximately 0.067 $/kWh, the infrared lamp concentrator system consumes approximately $0.0338 per kWh.

It is aimed to reduce electricity costs by storing 4 more hours of thermal energy with the electricity given in the charging state.

Table 9. Component and total cost values of the whole system

Product/material/process	Unit price [$]	Total price [$]
Infrared lamp 500 W	10	20
Furnace1 (stainless steel)	75	75
Furnace2 (glass)	10	10
Reflective foil	20	20
Metallic sheet	10	10
Quartz glass	20	20
Sodium Nitrate	2.5	25
Potassium Nitrate	3	30
Sodium Nitrite	2.5	25
Paraffin	3.5	35
Consumables and labour	30	30
Total [$]		300

In the system operating with Hitec salt, about 30% of the electricity consumed is stored as thermal energy, thus reducing electricity consumption costs. By spending approximately $0.134 for 0.5 kW of power over 4 hours, at least 0.8 kW of thermal energy is stored in 8 hours. Therefore, to convert the infrared ray concentrator system into useful work, it is sufficient to operate it for 4-6 hours instead of 8 hours. Additionally, the installation cost of the Hitec salt heat storage system was calculated to be $255. If the system operates for 12 hours a day, the installation cost is covered in approximately 2.5 years.

The installation cost of paraffin was calculated as $145. The amount of thermal energy stored in 8 hours with the paraffin heat storage system was obtained as an average of 0.32 kW. In order to convert this system into useful work, it is sufficient to run it for 4-6 hours instead of 8 hours. If the heat storage system with paraffin is operated for 12 hours a day, it can cover the installation cost in 1.7 years.

Thermoeconomic analysis was calculated as the ratio of the energy loss (Q_{loss}) of the whole system to the total heat storage system installation cost (Z_{inst}) [40]. The Thermoeconomic analysis of the whole system was calculated as 3.17 W/$ and 1.56 W/$ for paraffin and Hitec salt, respectively. In this case, it is seen that Hitec salt has less thermal energy loss and is more economical. On the other hand, using the same 500 W source for paraffin increased the thermal energy loss. It is recommended to use infrared light source with lower power for paraffin to prevent evaporation. Finally, in order to increase the Thermoeconomic efficiency of both storage systems, methods that increase heat transfer within the furnace should be used.

In this study, the operation and maintenance (O&M) cost of the infrared radiation thermal energy storage system was calculated to be approximately 97 $/kW per year. The thermal energy storage costs were determined to be 195 $/kWh for paraffin and 166 $/kWh for Hitec salt. In previous literature, it was reported that the O&M cost for the parabolic trough type thermal energy storage system with a power capacity of 100 MW, which can provide 6 hours of thermal storage with molten salts, ranged from 60 $/kW to 70 $/kW, while the thermal energy storage cost varied between 50 $/kW and 80 $/kWh [41]. It was found that the thermal energy storage costs per unit were

higher for small-scale storage systems than for large-scale systems. In this study, the capital costs were determined to be 3625 $/kW for paraffin and 2550 $/kW for Hitec salt, while the capital costs for trough-type thermal energy storage systems were reported to range from 6400 $/kW to 10,700 $/kW [42]. These results indicate that the capital costs of energy storage systems increase as their storage capacities grow.

5. Conclusions

Through the infrared lamp thermal energy storage system, sufficient temperatures were reached to melt the materials used, as confirmed by experimental and numerical methods. As a result, a new thermal energy storage method was tested. It was demonstrated that the heat transfers in the system, achieved through radiation and convection, made it safer by eliminating the risks of electrical conduction and short circuits, particularly in the salts within the furnace.

In the experiments for the Hitec salt charging condition, the focal temperature varied between approximately 280-300°C, while the average temperature of the upper region of the furnace was 220°C, and the temperature of the middle region of the furnace increased over time, reaching 87°C after 4 hours. On the other hand, after the 4-hour paraffin charging experiment, the focal temperature was recorded at 210°C, the upper region temperature at 80°C, and the middle region temperature at 22°C.

At the beginning of the discharge, the temperature of the Hitec salt was 102°C, and the temperature of the paraffin was 75.3°C. After 4 hours, the temperature of the Hitec salt dropped to 46°C, while the temperature of the paraffin decreased to 55.2°C. The slower cooling of paraffin was attributed to its lower thermal conductivity. The stability of Hitec salt at higher temperatures makes it highly suitable for medium and high-temperature applications.

The mass flow rates of the phase change materials in the furnace, measured using the infrared artificial ray method, were 0.047 g s^{-1} for paraffin and 0.061 g s^{-1} for Hitec salt, respectively. The average thermal efficiency of paraffin in the furnace was calculated to be approximately 56%, while the average thermal efficiency of Hitec salt was calculated to be 65.6%. Additionally, the first law of thermodynamics efficiency (total efficiency) for paraffin and Hitec salt was calculated to be 8% and 19.7%, respectively. As a result, paraffin is found to have a high heat storage capacity for low-temperature applications (up to around 80°C). However, for heat storage at medium and high temperatures, the Hitec salt mixture, an inorganic salt with a low melting point, high specific heat capacity, and stable operation at high temperatures, is considered more suitable.

The installation cost of the ray concentrator system is low. Additionally, the electricity required for the system can be supplied by a photovoltaic (PV) panel, making the system more economical. For high-temperature applications, such as those using Hitec salt, the reflective surface should be made of polished metal rather than foil to ensure temperature resistance. Finally, methods to improve heat transfer in the furnace should be developed to facilitate faster melting inside the furnace.

Acknowledgements

This article was financial supported give in by YÖK 100/2000 Project and TÜBİTAK BİDEB 2211-C. Also, this article is based on Ali Kemal Özcan's doctoral thesis completed in May 2024.

Author contributions

Ali Kemal Özcan: data curation, investigation, methodology, formal analysis, software, visualization; resources, writing-original draft, writing-review & editing.

Ömer Öksüz: data curation, investigation, visualization, roles/writing - original draft, writing - review & editing.

Cevdet Demirtaş: supervision, project administration, formal analysis, conceptualization, investigation.

References

1. Kraiem, M., Karkri, M., Fois, M., & Sobolciak, P., Thermophysical Characterization of Paraffins versus Temperature for Thermal Energy Storage, Buildings, **2023**, 13(4):877
2. Gallo, A., Marzo, A., Fuentealba, E., & Alonso, E., High flux solar simulators for concentrated solar thermal research: A review, Reviews, Renewable and Sustainable Energy 77, **2017**, 1385-1402
3. Ahmad, S., Hand, R., & Wieckert, C., Use of concentrated radiation for solar powered glass melting experiments, Solar Energy 109, **2014**, 174-182
4. Sarı, A., & Karaipekli, A., Thermal conductivity and latent heat thermal energy storage characteristics of paraffin/expanded graphite composite as phase change material, Applied Thermal Engineering, **2007**, 27(8-9):1271-1277
5. Akgun, M., Aydin, O., & Kaygusuz, K., Thermal energy storage behavior of a paraffin during melting and solidification. Energy Sources, Part A, **2007**, 29(14):1315-1326
6. Arslan, B., & Ilbas, M., A numerical study on the melting behaviors of paraffin with and without Al2O3 nanoparticles, Journal of Polytechnic, **2021**, 24(3): 1243-1248
7. Sinaringati, S., Putra, N., Amin, M., & Afriyanti, F., The utilization of paraffin and beeswax as heat energy storage in infant incubator, ARPN Journal of Engineering and Applied Sciences, **2016**, 11(2):800-804
8. Pedrosa, P., Marcelo, T., Nogueira, C.A., Gomes, A., & Diamantino, T., Molten nitrate salts containing lithium as thermal energy storage media: a short review, (ECOS) Proceedings of the 31st International Conference on Efficiency, Cost, Optimization, Simulation and Environmental Impact of Energy Systems, **2018**
9. Fernandez, A.G., Galleguillos, H., Fuentealba, E., & Perez, F.J., Thermal characterization of HITEC molten salt for energy storage in solar linear concentrated technology, Journal of Thermal Analysis and Calorimetry, **2015**, 122,3-9
10. Lingayat, A., Das, P., Gilago, M.C., & V.P., C. A detail assessment of paraffin waxed thermal energy storage medium for solar dryers, Solar Energy, **2023**, 261, 14-27
11. Chauhan, V., Yadav, A., & Soni, S., Simulation of Melting Process of a Phase Change Material (PCM) using ANSYS (Fluent), International Research Journal of Engineering and Technology (IRJET), **2017**, 04(05):3289-3294
12. Coastal Chemical Company, HITEC Heat Transfer Salt Houston, HITEC Heat Transfer Salt, **2011**
13. Ivenson, B., Broome, S., Kruizenga, A., & Cordaro, J. Thermal and Mechanical Properties of Nitrate St ate Thermal Storage Salts in the Solid-Phase, Solar Energy, **2012**, 86, 2897-2911

14. Dinçer, İ., & Rosen, M., Thermal energy storage: Systems and applications (2. edition), Hoboken, N.J.: Wiley, **2011**
15. Lane, G. A., and Lane, G.A. eds. Solar heat storage: latent heat materials. Vol. 1. Boca Raton, FL, USA: CRC press, **1983**
16. Sharma, A., Tyagi, V. V., Chen, C. R., & Buddhi, D., Review on thermal energy storage with phase change materials and applications, India: Renewable and Sustainable Energy Reviews, **2009**, 13(2):318-345
17. Subramaniam, S.B., & Senthil, R., Heat transfer enhancement of concentrated solar absorber using hollow cylindrical fins filled with phase change material, Interna tional journal of hydrogen energy, **2021**, 46(43):22344-22355
18. Sansaniwal, S. K., Sharma, V., & Mathur, J., Energy and exergy analyses of various typical solar energy applications: A comprehensive review, Renewable and Sustainable Energy Reviews, **2018**, 82, 1576–1601
19. Stine, W., & Diver, R., A Compendium of Solar Dish/Stirling Technology, California, US: Sandia National Laboratories, **1994**
20. Castellanos, L. M., Caballero, G. C., Cobas, V. M., Lora, E. S., & Reyes, A. M. Mathematical modeling of the geometrical sizing and thermal performance of a Dish/Stirling system for power generation. Renewable Energy, **2017**, 107, 23-35
21. Özcan, A.K., and Demirtaş, C., Obtaining high temperatures with ring array type (Rac) solar concentrators. 23rd Congress on Thermal Science and Technology with International Participation (ULIBTK'21), **2021**, 1, 640-646
22. Tetreault-friend, m., Gray, l., Berdibek, s., Mckrell, t., & Slocum, a., Optical properties of high temperature molten salt mixtures for volumetrically absorbing solar thermal receiver applications, Solar Energy, **2017**, 153, 238-248
23. Ambarita, H., Abdullah, I., Siregar, C.A., Siregar, R.E.T., Ronowikarto, A.D., Experimental Study on Melting and Solidification of Phase Change Material Thermal Storage, IOP Conference Series: Materials Science and Engineering, **2017**, 180, 012030
24. Xiao, X., Jia, H., Wen, D., & Zhao, X., Thermal performance analysis of a solar energy storage unit encapsulated with HITEC salt/copper foam/nanoparticles composite, Energy, **2020**, 192, 116593
25. Jaramillo, O. "Transporte de energía solar concentrada a través de fibras ópticas: acoplamiento fibra-concentrador y estudio térmico." Bachelor Thesis. Universidad Autónoma de Morelos. Estado de Morelos. México, **1998**
26. Ma, M., Ai, Q., and Xie, M. Optical properties of four types paraffin, Optik - International Journal for Light and Electron Optics, **2022**, 249, 168277
27. Astarita, T.; Carlomagno, G.M. Infrared Thermography for Thermo–Fluid–Dynamics, Springer: **2013**
28. Mark, F.H.; Kroschwitz, J.I. Encyclopedia of Polymer Science and Engineering; Wiley: New York, NY, USA, **1989**,17
29. Migliorino, M.T., Bianchi, D., and Nasuti, F., Numerical Simulations of the Internal Ballistics of Paraffin–Oxygen Hybrid Rockets at Different Scales, Aerospace, **2021**, 8(8): 213
30. Farnham, C., Nakao, M., Nishioka, M., and Nabeshima, M., Quantification of the Effect of Cooling Mists on Individual Thermal Comfort, The seventh International Conference on Urban Climate, **2009**
31. Xie, M., Zhu, Y., Liu, Y., Yuan, Y., and Tan, H., Measurement of spectral radiative characteristics of molten salt at high temperature using emission method, Applied Thermal Engineering **2019**, 149, 151–164
32. Darzi, A.A.R., Moosania, S.M. Tan, F.L., Farhadi, M., Numerical investigation of free-cooling system using plate type PCM storage, International Communications in Heat and Mass Transfer, **2013**, 48, 155–163
33. Zhang, P., Xiao, X., Meng, Z., & Li, M., Heat transfer characteristics of a molten-salt thermal energy storage unit with and without heat transfer enhancement. Applied Energy, **2015**, 137, 758–772
34. Voller, V., and Prakash, C., A Fixed-Grid Numerical Modeling Methodology for Convection-Diffusion Mushy Region Phase-Change Problems, Int. J. Heat Mass Transfer **1987**, 30, 1709 -1720
35. Hassab, M., Sorour, M., Mansour, M., and Zaytoun, M., Effect of volume expansion on the melting process's thermal behavior, Applied Thermal Engineering, **2017**, 115, 350–362
36. Kline, S., and McClinton, F., Describing Uncertainties in Single-Sample Experiment, Mechanical engineering, **1953**, 75, 3-9
37. Sinaringati, S., Putra, N., Amin, M., and Afriyanti, F., The utlization of paraffin and beeswax as heat energy storage in infant incubator, ARPN Journal of Engineering and Applied Sciences, **2016**, 11(2):800-804
38. Bellan, S., Alonso, E., Gomez-Garcia, F., Perez-Rabago, C., Gonzalez-Aguilar, J., Romero, M., Thermal performance of lab-scale solar reactor designed for kinetics analysis at high radiation fluxes, Chemical Engineering Science, **2013**, 101, 81–89
39. Kuhn, P., and Hunt, A., A new solar simulator to study high temperature solid-state reactions with highly concentrated radiation, Solar Energy Materials, **1991**, 24, 742–750
40. Rosen, M., and Dincer, I., Exergoeconomic analysis of power plants operating on various fuels, Applied Thermal Engineering **2003**, 23, 643–658
41. Turchi, C., Mehos, M., Ho, C. K.& Kolb, G. J. Current and future costs for parabolic trough and power tower systems in the US market, Conference paper NREL CP, **2010**, 5500-49303
42. Roubaud, E. G., Pérez-Osorio, D., Prieto, C. Review of commercial thermal energy storage in concentrated solar power plants: Steam vs. molten salts, Renewable and Sustainable Energy Reviews, **2017**, 80, 133–148